

Journal of Chemical, Biological and Physical Sciences



An International Peer Review E-3 Journal of Sciences

Available online at www.jcbps.org

Section A: Chemical Sciences

CODEN (USA): JCBPAT

Research Article

Performance of azafuramidine derivatives as new corrosion inhibitors for CS in acid environment: The Experimental and Quantum chemical studies

A. S. Fouda, M. A. Ismail, M. N. EL-Haddad*, A. Abd Elgyed

Chemistry Department, Faculty of Science, Mansoura University, Mansoura-35516, Egypt

Received: 28 June 2018; Revised: 15 July 2018; Accepted: 28 July 2018

Abstract: Three azafuramidine derivatives (AZFD) as new inhibitors for the corrosion of carbon steel (CS) in acidic solution has been examined by mass loss (ML), atomic absorption spectroscopy (AAS) and electrochemical techniques. The results demonstrated that these new (AZFD) act as good inhibitors for the corrosion of CS in acidic media. The inhibition efficiency (% ϵ) increased as the inhibitor concentrations increases. Potentiodynamic polarization (PP) study showed that (AZFD) may be classified as mixed-type inhibitors. The adsorption of (AZFD) on metal surface showed a Langmuir isotherm route. The surface analysis of the CS was investigated using ATR-FTIR, UV/visible spectroscopy and AFM analysis. Surface analysis of CS revealed formation of a protective adsorbed surface layer composed of (AZFD). Quantum chemical calculations of the azafuramidine derivatives molecules were computed and discussed.

Keywords: CS, AZFD, HCl, AFM, DFT

1. INTRODUCTION

CS is a common metal used to produce and transport crude oil in oil wells. This is attributed to its good mechanical properties. During the transfer of crude oil through the pipelines, occurs direct contact between metal and migrating ions due to the breakdown of the oil aqueous emulsion, which leads to the

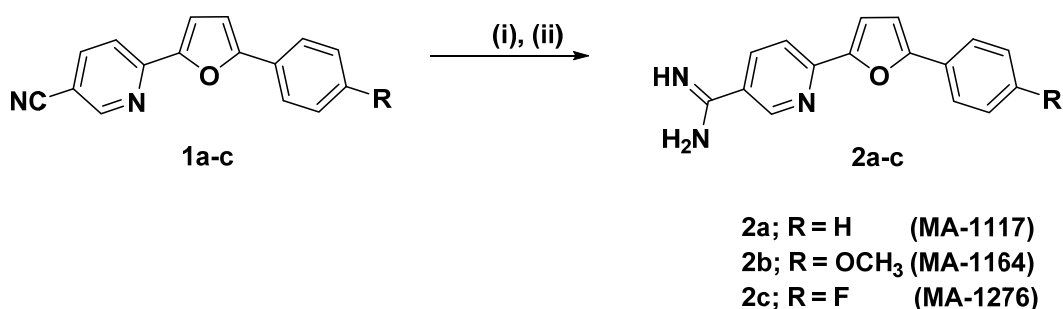
metal corrosion. Consequently, many researchers have tended to use organic compounds as corrosion inhibitors for CS in acidic media¹⁻¹².

The corrosion rate of CS is decreased when these inhibitors added to the corrosive media. So, the adsorption of inhibitors molecules onto metal/solution interface is affected by (1) electrostatic interaction between charged CS surface and charged inhibitor molecules, (2) lone pair electrons of heteroatoms (O, N or S) interacting with vacant d-orbitals of Fe atoms in the CS, (3) π -electrons in aromatic rings interacting with vacant d-orbital of Fe atoms in the metal and when possible, (4) a combination of some of these three interactions. Recently, furan-containing molecules proved to be good corrosion inhibitors due to their structures features that enable them to bind effectively to CS surface¹³. In our present work, we will study three (AZFD) as new corrosion inhibitors for CS in acidic solution. These derivatives are nontoxic, safe and eco-friendly corrosion inhibitors, in addition to their significant antibacterial and ant proliferative activities¹⁴. The inhibition efficiency of (AZFD) for the CS corrosion in acidic media was investigated using (ML), (AAS), (PP), (EFM) and (EIS) techniques. The analysis of surface was used to characterize the CS surface without and with the inhibitors. Quantum chemical study was discussed using DFT method to support the experimental data. A good agreement was observed in the results of experimental and theoretical measurements. The order of investigated three (AZFD) according to inhibition efficiency showed that, MA-1164 > MA-1276 > MA-1117.

2. MATERIAL AND METHODS

2.1. Solutions and materials: The CS chemical composition used in all testing methods was (wt %): Mn (0.39), Si (0.19), C (0.12), P (0.41), S (0.05), Cu (0.024) and the rest is iron. The coupons required for ML, AAS, ATR-FTIR, and AFM measurements were cut into one size. Prior the tests, the surface of CS coupons were polished with different emery papers up to 1200 grade, cleaned up via multiple washing using bi-distilled water. Cleaned samples were stored at room in a vacuum desiccator until use.

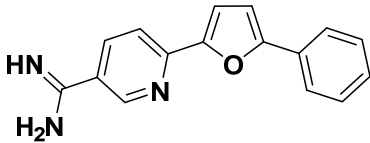
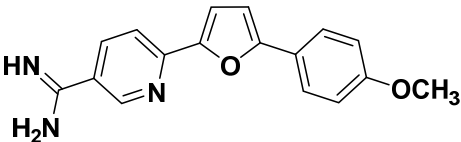
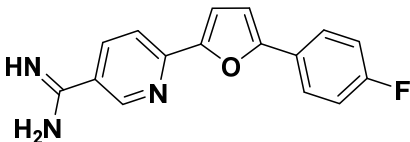
The inhibitor concentrations were (1-21 μ M). The synthetic route of the investigated (AZFD) is shown in **Scheme 1**, and the molecular structures is given in **Table 1**. The details for the synthesis and structural elucidation, including spectral data (FTIR, Mass, NMR) of these azafuramidines **2a-c** have been recently reported [14].



Scheme 1: Synthetic route for azafuramidines **2a-c**.

Reagents and conditions: (i) Lithium bis-(trimethylsilyl)amide, ii) ethanol/hydrogen chloride

Table 1. Chemical structures of the investigated (AZFD)

Inhibitor Code	Molecular structures/Chemical names	Mol. Formulas/(Mol.Wt.)
MA-1117	 6-(5-Phenylfuran-2-yl)nicotinamide	C ₁₆ H ₁₃ N ₃ O·2.0HCl (336.21)
MA-1164	 6-[5-(4-Methoxyphenyl)furan-2-yl]nicotinamide	C ₁₇ H ₁₅ N ₃ O ₂ ·2.0HCl·0.75H ₂ O (379.75)
MA-1276	 6-[5-(4-Fluorophenyl)furan-2-yl]nicotinamide	C ₁₆ H ₁₂ FN ₃ O·2.0HCl·0.5H ₂ O (363.21)

2.2. Mass loss (ML) technique: The dimensions of abraded CS samples 2 x 2 x 0.1 cm were weighed before immersion in test solution without and with different concentrations of (AZFD) at required temperature, using water bath. The CS coupons after every 30 minutes were taken out from the test solution, rinsed with bi-distilled water, then carefully dried and re-weighed. The total immersion time was 180 minutes. The ML (mg cm⁻²) was obtained as difference between the initial and final weight of CS specimen.

2.3. Atomic absorption spectroscopy (AAS) measurements: The abraded CS specimens were immersed in test medium with and without various concentrations of (AZFD) for one day at 298 ± 1 K. The amount of metal ion dissolved in the acidic solution was determined using atomic absorption spectrometer (model Sens AA, GBC Scientific Equipment, USA).

2.4. Electrochemical technique: The measurements of electrochemical technique were performed using Potentiostat-Galvanostat-ZRA analyzer (Gamry-PCI4G750, Warminster, PA, USA). The experimental data were analyzed and fitted using E-chem Analyst 5.5 software. The electrochemical cell used in this study, includes CS as a working electrode (WE) with an area (1.0 cm²) immersed in test solution, sheet of platinum as a counter electrode (CE), and a saturated calomel electrode (SCE) as a reference electrode.

(RE). Before recording the electrochemical measurements, the WE was immersed in corrosive medium and allowed to corrode freely for 30 min at room temperature of 298 ± 1 K, to attain steady state, during which its open circuit potential (OCP) was measured as a function of time. PP was measured in the potential range from (+250 to -250 mV) from the OCP at the scan rate (0.5 mV s^{-1}). EFM technique was performed using the frequencies (2.0 and 5.0 Hz). The base frequency was 0.1 Hz and 10 mV potential disturbance signals. On the other hand, EIS technique was carried out using the frequency range from (100 kHz to 10 mHz) with 10 mV peak to peak voltage excitation and 5.0 mV a signal amplitude perturbation at OCP. EIS data were fit to suitable equivalent circuits (ECs) using the E-chem Analyst software.

2.5. Atomic force microscopy (AFM) analysis: The coupons of CS were treated in the same manner of ML method, and immersed in test solution without and with concentration ($21 \mu\text{M}$) of azafuramidine derivatives for 24 hrs at 298 ± 1 K. After this period, the coupons were taken out, carefully rinsed using bi-distilled water, and dried. Then, the surface analysis of CS was investigated using AFM (Nano surf Flex) system.

2.6. ATR-FTIR and UV/visible spectral analysis: ATR-FTIR measurement gives a qualitative guide to the adsorption of inhibitor on the CS surface. The surface of CS coupons immersed in the test solution without and with the inhibitors was analyzed directly by single reflection mode using (Thermo Fisher Nicolet iS10, USA). UV/visible spectra of $21 \mu\text{M}$ of investigated inhibitors and the test solution containing inhibitors after immersion of CS coupons for 24 h measured on (T80+ UV/VIS spectrometer, UK).

2.7. Quantum chemical studies: In this work, quantum chemical studies were performed using (Gaussian program package, version 9.0, Pittsburgh, PA, USA) by DFT method. The calculated quantum chemical parameters were visualized using (Gauss View 3.0) in the liquid state, because the corrosion process occurs in the solution medium.

RESULTS AND DISCUSSION

3.1. ML tests

3.1.1. influence of inhibitor concentrations : ML measurements were performed to show the influence of inhibitor concentrations on the rate of corrosion (C_R) of CS in 1.0 M HCl medium, (C_R) and inhibition efficiency ($\% \epsilon_{ML}$) were obtained using the following relations¹⁵:

$$C_R = \frac{W_I - W_F}{AT} \quad (1)$$

$$\% \epsilon_{ML} = \left[1 - \frac{C_R}{C_R^*} \right] \times 100 \quad (2)$$

Where W_I and W_F are the initial and final weight of CS sample (mg), A is the CS surface area (cm^2), t is the immersion time of CS in test solution (hours), and C_R^* and C_R are the CS corrosion rate ($\text{mg}/\text{cm}^2\text{h}$) without and with of inhibitor concentration, respectively.

The effect of various concentrations of (AZFD) on the C_R and $\% \epsilon_{ML}$ of CS corrosion in test solution at 298 ± 1 K are shown in **Figure 1**. It's obvious that, the existence of inhibitor in the corrosive solution leads to a decrease in C_R and on the other hand, increase $\% \epsilon_{ML}$. And therefore, the adsorption of inhibitor molecules on the surface of CS, leads to the formation of a protective adsorbed layer on the surface,

which retard the anodic and cathodic reaction sites in the test solution of corrosion. From ML data in **Table 2**, it is found that, the order of the investigated azafuramidines according to % ϵ_{ML} was in the sequence as follow: MA-1164 > MA-1276 > MA-1117.

Table 2. Influence of various concentrations of (AZFD) on the C_R and % ϵ_{ML} of CS in 1.0 M HCl solution at different temperatures ((immersion time 120 minutes)

Temp, K	298		303		308		313		318	
Conc., μM	$C_R \times 10^{-3}$ $\text{mgcm}^{-2}\text{min}^{-1}$	% ϵ_{ML}	$C_R \times 10^{-3}$ $\text{mgcm}^{-2}\text{min}^{-1}$	% ϵ_{ML}	$C_R \times 10^{-3}$ $\text{mgcm}^{-2}\text{min}^{-1}$	% ϵ_{ML}	$C_R \times 10^{-3}$ $\text{mgcm}^{-2}\text{min}^{-1}$	% ϵ_{ML}	$C_R \times 10^{-3}$ $\text{mgcm}^{-2}\text{min}^{-1}$	% ϵ_{ML}
Blank	15.55	----	20.0	----	24.73	----	38.68	----	50.0	----
MA-1164										
1	5.58	64.1	5.78	71.1	6.68	72.9	8.56	78.0	10.4	79.1
5	3.58	71.0	4.20	79.0	4.73	80.8	6.58	83.0	7.0	86.0
9	3.48	77.5	3.62	81.9	4.15	83.2	4.98	87.1	5.2	89.6
13	2.84	81.7	3.02	84.8	3.39	86.3	3.59	90.7	4.0	92.8
17	2.49	84.	2.89	85.5	3.11	87.4	3.18	91.7	3.2	93.6
21	2.29	85.2	2.60	86.9	2.69	89.1	2.79	92.8	2.99	94.0
MA-1276										
1	5.65	63.4	6.60	66.9	7.67	68.9	9.09	76.5	10.9	78.2
5	3.98	74.3	4.78	76.1	4.96	79.9	6.18	84.0	7.27	85.4
9	3.69	76.2	4.34	78.2	4.73	80.8	5.28	86.3	6.18	87.6
13	3.31	78.7	3.85	80.7	4.27	82.7	4.36	88.7	5.11	89.8
17	3.29	78.8	3.62	81.9	4.03	83.6	4.18	89.2	4.88	90.2
21	3.09	80.1	3.11	84.4	3.55	85.6	3.79	90.2	4.18	91.6
MA-1117										
1	5.96	61.6	7.15	64.2	8.78	64.5	10.4	73.1	12.6	74.8
5	4.88	68.5	5.79	71.0	6.23	74.8	8.17	78.8	8.87	82.2
9	4.58	70.5	5.50	72.4	5.70	76.9	6.28	83.7	7.67	84.6
13	4.07	73.8	4.54	77.2	4.60	81.4	5.68	85.3	7.10	85.8
17	3.58	76.9	4.20	79.0	4.27	82.7	5.08	86.8	5.98	88.0
21	3.19	79.4	3.91	80.4	4.15	83.2	4.68	87.9	5.18	89.6

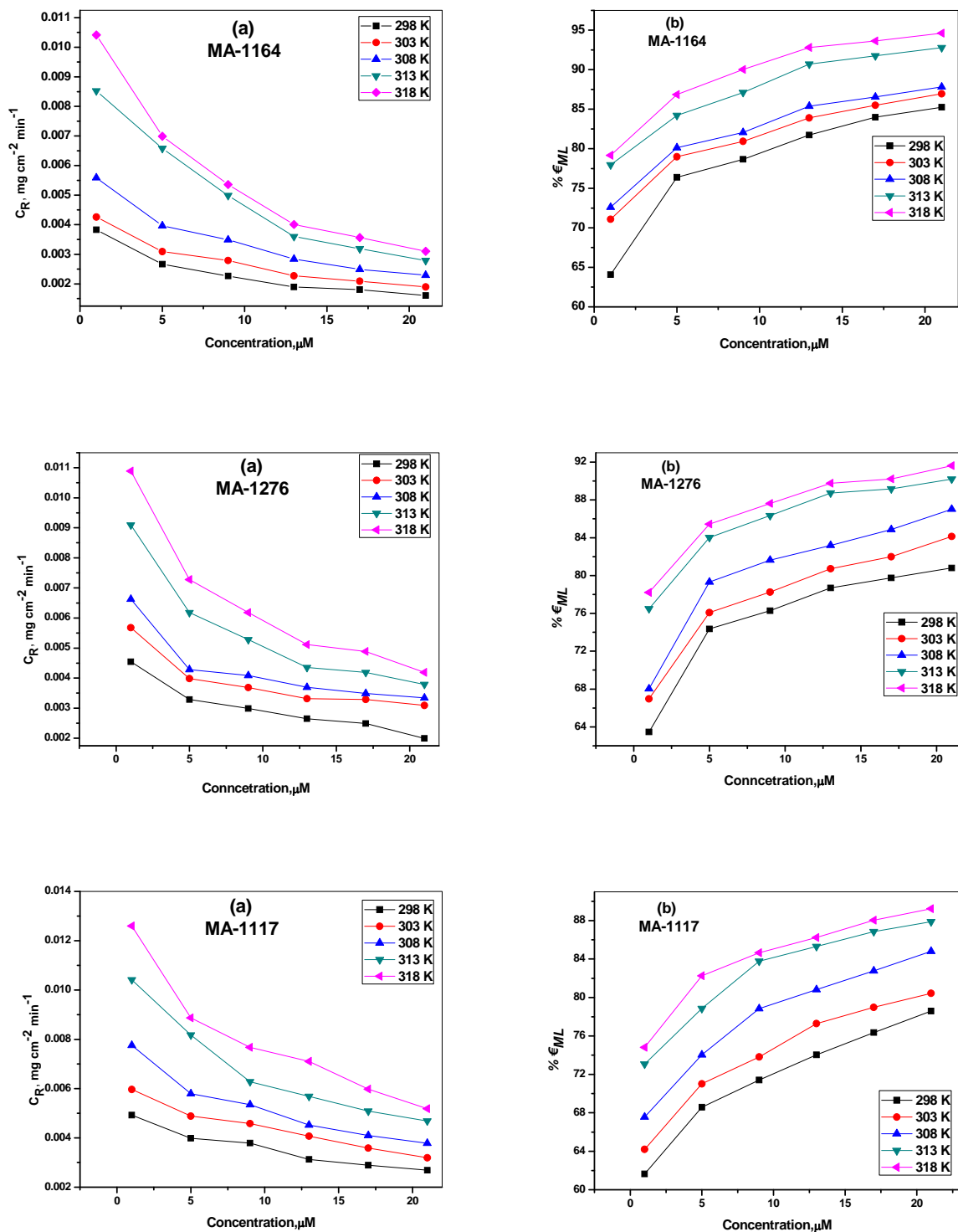


Fig. 1: Influence of various concentrations of (AZFD) on the C_R (a) and $\% \epsilon_{ML}$ (b) of CS corrosion in 1.0 M HCl solution at (298 - 318 K)

3.1.2. Influence of temperature and activation parameters: The temperature effect on C_R and % ϵ_{ML} of CS in test medium with and without different concentrations of (AZFD) was studied at 298–303K, and the C_R and % ϵ_{ML} obtained are summarized in **Table 2**. The C_R is related to the temperature and activation energy (E_a^*) as described through the following Arrhenius relation:

$$\log C_R = \log \lambda - \left(\frac{E_a^*}{2.303RT} \right) \quad (3)$$

Where λ is Arrhenius pre-exponential factor, R is molar gas constant and T is absolute thermodynamic temperature (K).

Arrhenius plots ($\log C_R$ against $1/T$) for dissolution of CS in test solution with and without various concentrations of (AZFD) are given in **Figure 2a**. The E_a^* values were calculated from the slopes of the straight lines (**Figure 2a**), and listed in **Table 3**. The C_R is related to the temperature by alternate form of the Arrhenius relation as follow:

$$\frac{\log C_R}{T} = \log \frac{R}{Nh} - \frac{\Delta H^*}{2.303RT} + \frac{\Delta S^*}{2.303R} \quad (4)$$

Where 'N' is number of Avogadro, 'h' is constant of Planck, ΔH^* and ΔS^* are the changes of enthalpy and entropy of activation, respectively.

Plots $\log (C_R/T)$ against $(1/T)$ for dissolution of CS in test solution in without and with various concentrations of (AZFD) are given in **Figure 2b**. The values of ΔH^* and ΔS^* obtained from the slopes and the intercepts of straight lines of **Figure 2b**, and recorded in **Table 3**.

It is found that, E_a^* and ΔH^* values in case of test solution containing inhibitors are higher than the solution without inhibitors (blank). So, the rate determining steps of metal dissolution and evolution of hydrogen are associated with higher energy barrier in the existence of (AZFD) molecules. This is due to increase the CS surface coverage by the inhibitor molecules, which inhibit the anodic and cathodic active sites, add to that increase in the thickness of the adsorbed layer, which protect the CS surface from corrosive solution¹⁶.

Additionally, a positive value of ΔH^* indicated that the corrosion of CS in acidic solution is endothermic process. On the other hand, A negative values of ΔS^* revealed that the formation of activated complex is an associative step rather dissociative. It is clear that, the values of ΔS^* are more negative in case of uninhibited test solution than inhibited solution. This is due to the replacement of H_2O molecules from the surface of the metal by the inhibitor molecules¹⁷.

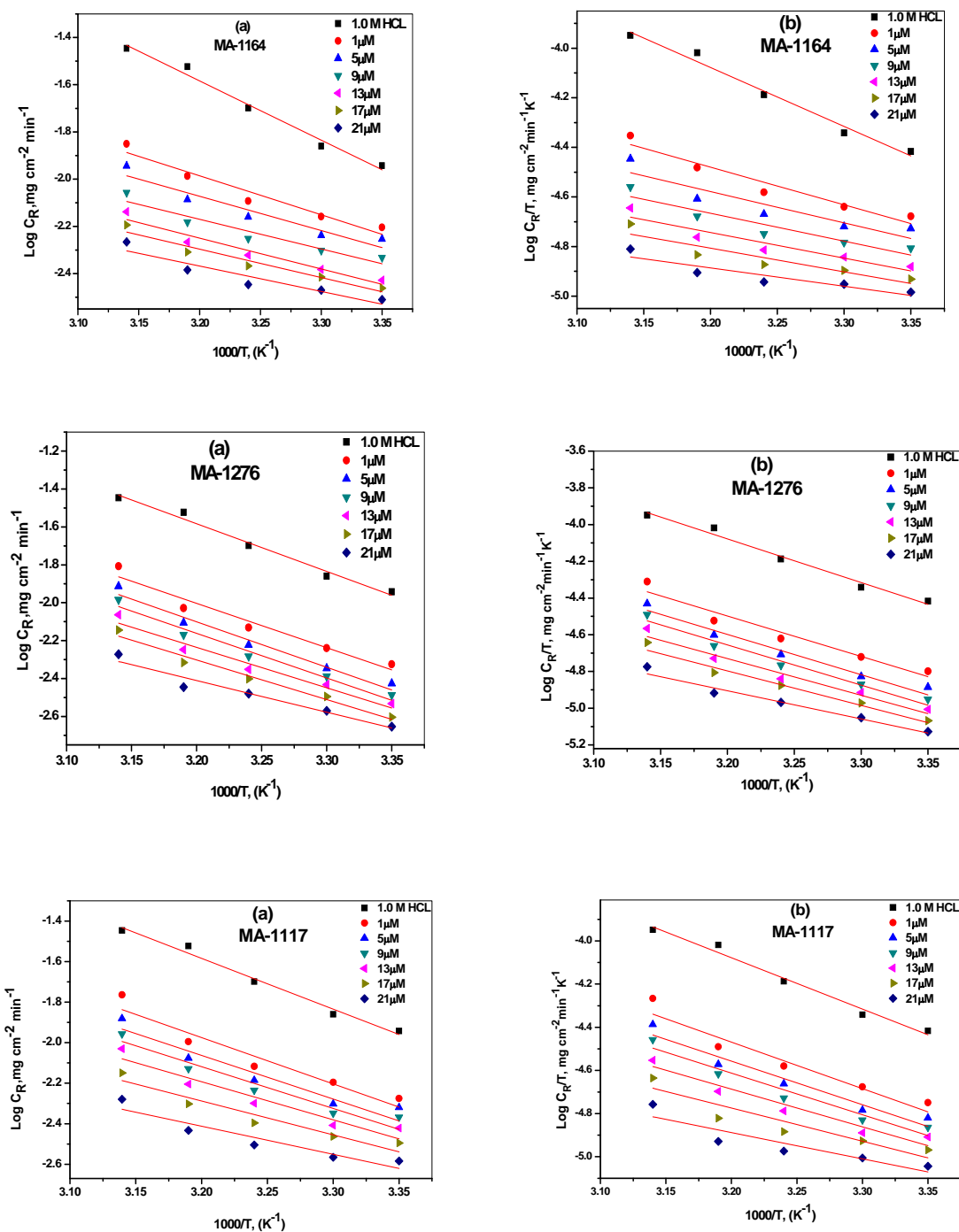


Fig.2: Arrhenius plots ($\log C_R$ against $1/T$) (a), and plot ($\log C_R/T$ against $1/T$) (b) for dissolution of CS in 1.0 M HCl solution without and with different concentrations (AZFD)

Table 3: Kinetic parameters obtained from ML measurements for CS dissolution in 1.0 M HCl solutions in absence and presence of different concentrations of (AZFD)

Conc., μM	E_a^* , kJ mol^{-1}	ΔH^* , kJ mol^{-1}	$-\Delta S^*$, $\text{J mol}^{-1}\text{K}^{-1}$
Blank	12.51	14.10	245.87
MA-1164			
1	23.02	32.54	186.33
5	24.10	38.98	163.79
9	25.03	41.39	154.65
13	27.73	43.25	147.14
17	31.62	45.53	129.84
21	48.09	55.05	105.29
MA-1276			
1	22.95	29.40	197.27
5	23.44	35.91	174.39
9	24.46	38.22	165.70
13	26.95	41.83	152.71
17	30.66	42.19	148.57
21	44.75	47.29	132.66
MA-1117			
1	19.33	23.30	216.49
5	20.12	33.40	180.29
9	22.76	36.94	167.54
13	23.12	38.67	160.95
17	28.86	41.31	150.83
21	35.93	45.53	129.84

3.1.3. Adsorption isotherm and thermodynamic parameters: The adsorption of (AZFD) molecules can either occur chemically or physically on the corroded CS surface. The degrees of surface coverage (θ) for various concentrations of (AZFD) in test solution were obtained from the ML measurements, and were fitted with different adsorption isotherm models. Straight lines (**Figure 3**) were obtained on plotting C_{inh}/θ versus concentrations of inhibitors (C_{inh}) at different temperatures (298-303K), revealing that the inhibitor adsorption on the metal surface follows Langmuir adsorption isotherm, which has the following relation:

$$\frac{C_{inh}}{\theta} = C_{inh} + \frac{1}{K_{ads}} \quad (5)$$

Where ' K_{ads} ' is the equilibrium constant of adsorption process, which is related to the free energy of adsorption (ΔG_{ads}^0), according to following relation¹⁸:

$$\Delta G_{ads}^0 = -RT \ln(10^6 K_{ads}) \quad (6)$$

Where ' 10^6 ' is concentration of H_2O molecules in the test solution (mgL^{-1}).

On the other hand, ΔG_{ads}^0 is related to the enthalpy (ΔH_{ads}^0) and the entropy (ΔS_{ads}^0) of adsorption and the according to Gibbs–Helmholtz relation as follow¹⁹:

$$\Delta G_{ads}^0 = \Delta H_{ads}^0 - T\Delta S_{ads}^0 \quad (7)$$

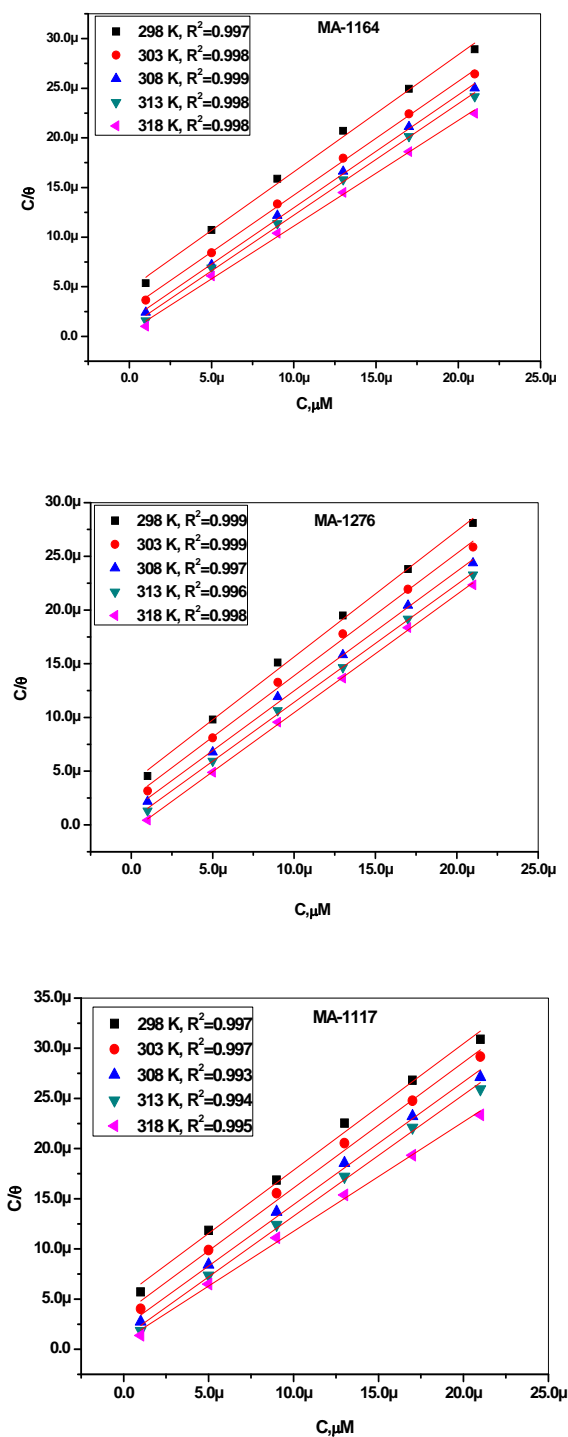


Fig. 3: Langmuir adsorption isotherm plot of C/θ versus C for CS corrosion in 1.0 M HCl solution containing various concentrations of (AZFD) at different temperatures

Plots of ΔG_{ads}^0 versus T for CS corrosion in presence of different (AZFD) give straight lines as shown in Figure 4. ΔS_{ads}^0 and ΔH_{ads}^0 can be obtained from the slope and the intercept of the straight lines (**Figure 4**), respectively. The thermodynamic adsorption parameters for (AZFD) on the surface of CS are summarized in **Table 4**. It is found that, the values of K_{ads} are increasing with temperature, suggesting that a strong interaction between (AZFD) molecules and the CS surface in acidic medium. In addition, large values of (K_{ads}) calculated for the investigated (AZFD) revealed that the adsorption process is more efficient thus improving the corrosion inhibition efficiency. The values of ΔG_{ads}^0 are negative and more than - 40 kJ/mol suggested that, the adsorption mode of (AZFD) on the surface of metal is a spontaneous process and chemisorption adsorption. The positive sign of ΔH_{ads}^0 value points out the adsorption of (AZFD) on the metal surface is endothermic because of chemisorption process ²⁰. On the contrary, ΔS_{ads}^0 positive values reflect the increase in the entropy of solvent as disorder occurs at the CS/solution interface when the (AZFD) molecules adsorbed on the CS surface. This is due to the displacement of H_2O molecules by (AZFD) molecules on the CS surface in the corrosive medium ¹³.

Table 4: Thermodynamic parameters obtained from ML measurements for CS dissolution in 1.0 M HCl solutions containing various concentrations of (AZFD) at different temperatures

Inhibitor	Temp., K	$K_{\text{ads}} \times 10^{-4}$, M^{-1}	$-\Delta G_{\text{ads}}^0$, kJ mol^{-1}	ΔH_{ads}^0 , kJ mol^{-1}	ΔS_{ads}^0 , $\text{J mol}^{-1} \text{K}^{-1}$
MA-1164	298	93.01	44.01	16.89	203.53
	303	96.73	44.84		
	308	104.62	45.78		
	311	117.73	46.83		
	318	143.08	48.10		
MA-1276	298	56.37	42.76	32.77	252.99
	303	65.82	43.87		
	308	74.02	44.90		
	311	97.13	46.33		
	318	130.73	47.86		
MA-1117	298	38.27	41.80	37.97	267.53
	303	49.50	43.15		
	308	56.02	44.18		
	311	78.27	45.77		
	318	101.31	47.18		

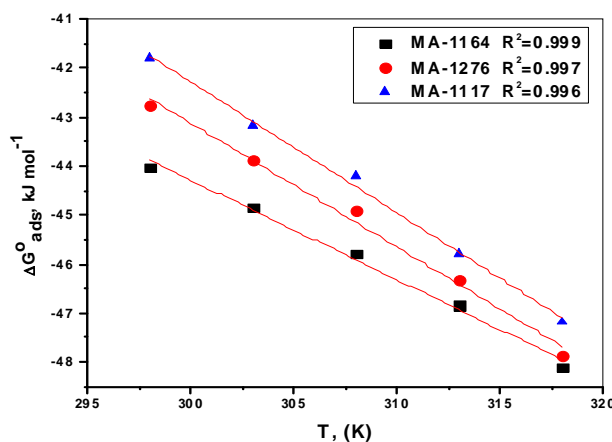


Fig. 4: Plots of $\Delta G_{\text{ads}}^{\circ}$ versus T for CS corrosion in presence of different (AZFD)

3.2. AAS measurements: AAS is a quantitative analysis method was used to determine the amount of dissolved Fe in the corrosive medium with and without various concentrations of (AZFD) at required temperature. The $\% \epsilon_{\text{AAS}}$ was calculated according to the following relation:

$$\% \epsilon_{\text{AAS}} = \left[1 - \frac{A}{A^*} \right] \times 100 \quad (8)$$

Where A^* and A are the amount of dissolved iron in test medium without and with inhibitor, respectively. Amount of dissolved iron in test solution measured using AAS is summarized in **Table 5**. It is found that the amount of dissolved Fe in case of the inhibited solution is lower than the uninhibited solution (blank). There was a delay in the dissolution of metal in corrosive medium because of formation of adsorbed layer of (AZFD) on the CS surface²¹. It is found that, the order of $\% \epsilon_{\text{AAS}}$ for investigated (AZFD) according to the amount of dissolved Fe in the corrosive medium showed that $\text{MA-1164} > \text{MA-1276} > \text{MA-1117}$.

Table 5. Amount of iron dissolved in 1.0 M HCl solution without and with different concentrations of (AZFD) at 298K (immersion time 24h)

Conc., μM	Amount of iron, $\mu\text{g/L}$	$\% \epsilon_{\text{AAS}}$
Blank	13.51	-----
MA-1164		
1	3.63	73.1
5	3.20	76.3
9	2.67	80.2
13	2.07	84.7
17	1.59	88.2
21	1.22	91.0

MA-1276		
1	4.50	66.7
5	3.86	71.4
9	3.13	76.8
13	2.51	81.4
17	2.01	85.1
21	1.62	88.0
MA-1117		
1	5.21	61.4
5	4.49	66.8
9	3.86	71.4
13	3.23	76.1
17	2.65	80.4
21	2.09	84.5

3.3. Electrochemical techniques

3.3.1. PP test: PP plots ($\log i_{\text{corr}}$ versus E_{corr}) for CS corrosion in test medium without and with various concentrations of (AZFD) are represented in **Figure 5**. The corrosion parameters (i_{corr} , E_{corr} , β_a and β_c) calculated from PP method are recorded in **Table 6**. The % ϵ_{pp} obtained from pp method was calculated using the relation as follow [22]:

$$\% \epsilon_{pp} = \left(\frac{i_{\text{corr}} - i_i}{i_{\text{corr}}} \right) \times 100 \quad (9)$$

Where i_{corr} and i_i is corrosion current density without and with inhibitor concentration, respectively.

As shown from **Figure 5**, the cathodic and anodic reactions of CS were affected after addition of (AZFD) to test solution. So, the additions of (AZFD) decrease the corrosion of CS and delay the hydrogen evolution reaction. From **Table 6**, the values of i_{corr} reduce with increase in inhibitor concentration, and hence, % ϵ_{pp} values increase. It is found that, there is a slight shift in corrosion potential, with no definite trend in the shift of E_{corr} values with increase in inhibitor concentrations compared to that of blank solution.

This due to the inhibitors has mixed effectiveness by impeding the anodic and cathodic reaction centers on CS surface (i.e. (AZFD) act as mixed-type inhibitors)²³. The cathodic and anodic Tafel slopes (β_c and β_a) change when the inhibitor added to the test solution. This points out that the anodic and cathodic reaction sites are delayed with change in their mechanisms. The order of investigated compounds according to % ϵ_{pp} is an agreement with the % ϵ_{ML} values calculated from ML and AAS techniques, whereas: MA-1164 > MA-1276 > MA-1117.

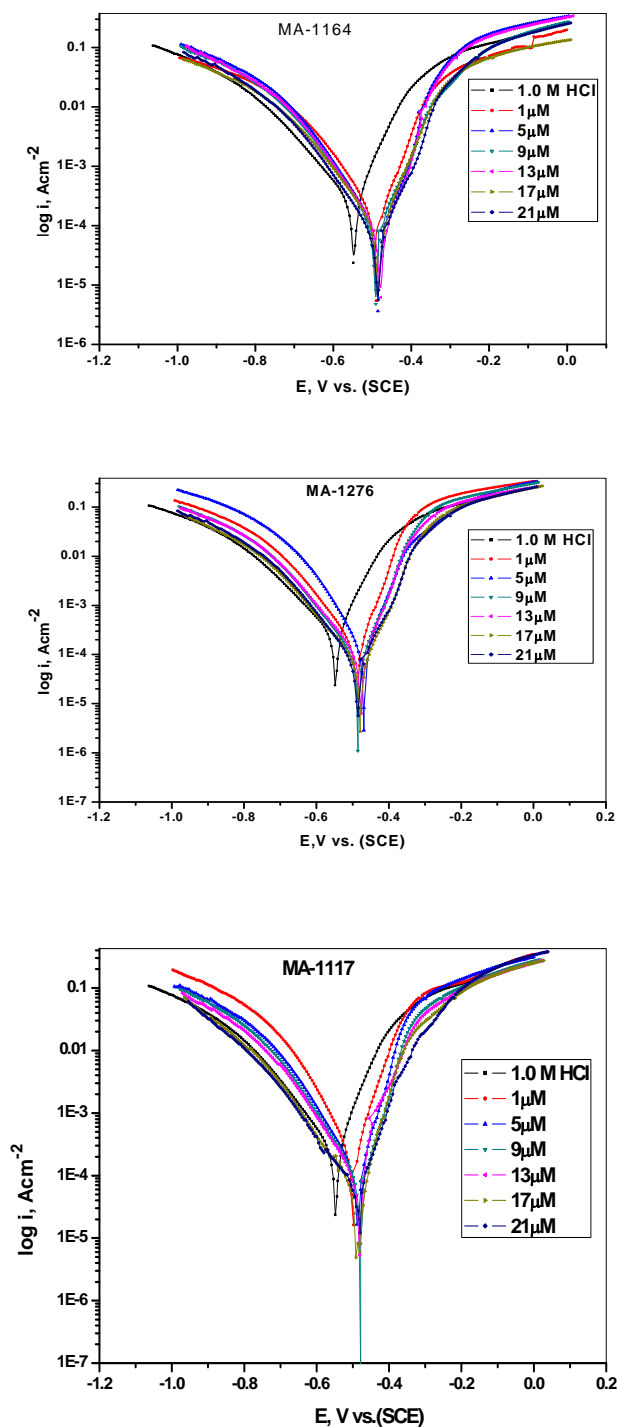


Fig. 5: PP plots ($\log i_{\text{corr}}$ versus E_{corr}) for CS electrode in uninhibited and inhibited solutions with various concentrations of (AZFD) at 298 K

Table 6:PP kinetic parameters for CS dissolution in 1.0 M HCl without and with different concentrations of (AZFD) at 298 K

Conc., (μM)	i_{corr} , (μAcm^{-2})	$-E_{\text{corr}}$, (mV vs SCE)	β_a , (mV dec $^{-1}$)	β_c , (mV dec $^{-1}$)	C_R , (mpy)	% ϵ_{PP}
Blank	433	547	100	180	198	-----
MA-1164						
1	161	490	69.9	118.3	73.66	62.80
5	145	492	90.1	134.2	66.33	66.50
9	110	485	72.9	131.6	41.58	79.00
13	83.9	486	64.5	108.5	38.41	80.60
17	80.3	479	61.9	119.9	36.6	81.50
21	67.3	486	72.5	115.5	30.5	84.46
MA-1276						
1	238	499	89.7	128.3	108.9	45.00
5	226	488	70.5	140.1	103.5	47.80
9	117	477	70.8	130.4	54.85	72.30
13	108	485	67.8	130.5	49.3	75.10
17	84.7	464	69.9	165.7	38.8	80.40
21	76.9	479	73.2	134.4	35.2	82.24
MA-1117						
1	255	469	61.5	128.5	116.6	41.10
5	240	499	63.9	111	109.7	44.60
9	124	482	66.6	137.9	56.63	71.40
13	115	484	66.1	127.2	52.67	73.40
17	102	478	60.5	134.5	46.7	76.40
21	85.3	479	65.0	143.4	39.6	80.30

3.3.2. EFM measurements: EFM intermodulation spectra of CS dissolution in test solution with and without (AZFD) at 298 K are displayed in **Figure 6**. The inhibition efficiency (% ϵ_{EFM}) obtained from EFM technique was calculated using the relation as follow:

$$\% \epsilon_{\text{EFM}} = \left(\frac{i_{\text{corr}} - i_i}{i_{\text{corr}}} \right) \times 100 \quad (10)$$

The corrosion parameters obtained from EFM method are shown in **Table 7**. It is found that, i_{corr} decrease with increasing (AZFD) concentrations, and therefore, % ϵ_{EFM} values increase. The causality factors (CF-2 and CF-3) are found close to the standard values (2.0 and 3.0), and therefore, the data obtained from this technique are valid²². The % ϵ_{EFM} obtained from EFM technique is the same sequence of ML, AAS and PP methods whereas: MA-1164 > MA-1276 > MA-1117.

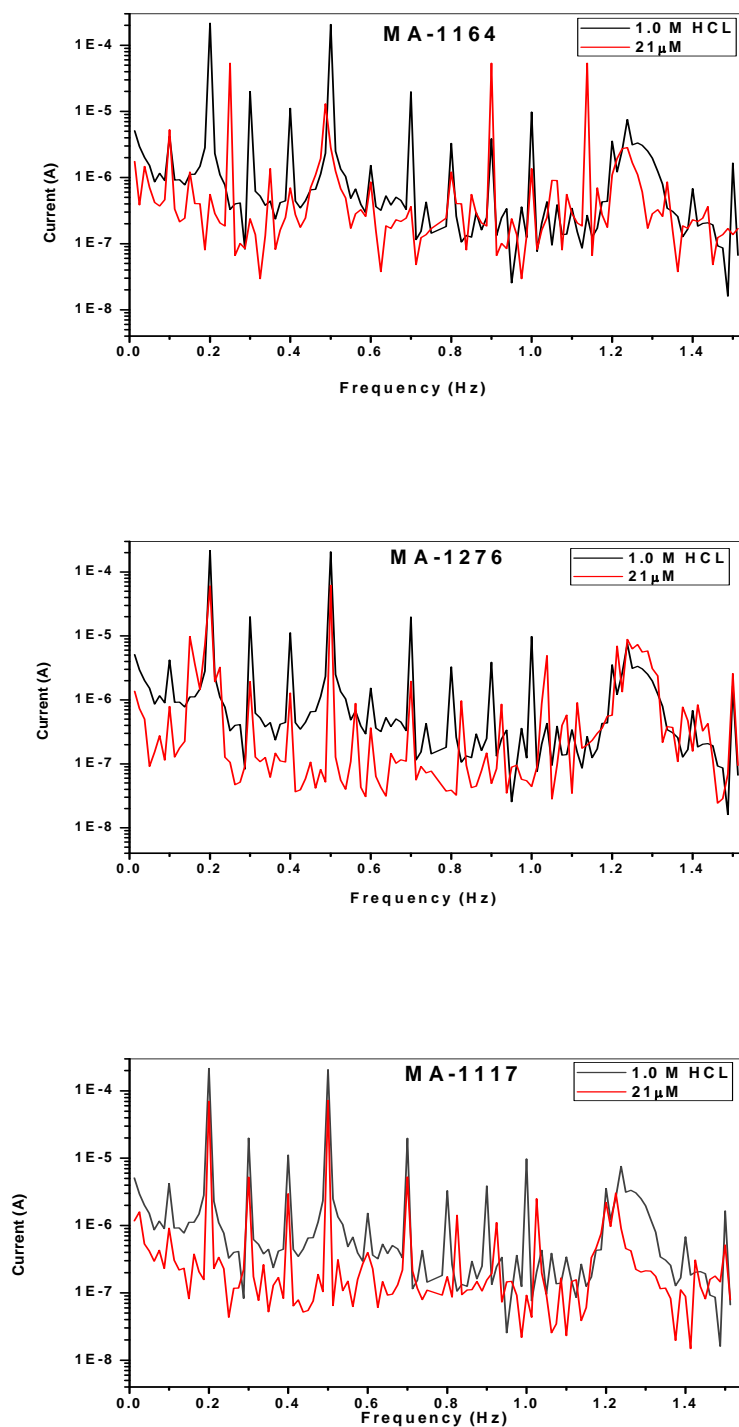


Fig. 6: The intermodulation spectra of CS dissolution in 1.0 M HCl solution without and with 21 μ M of (AZFD) at 298 K

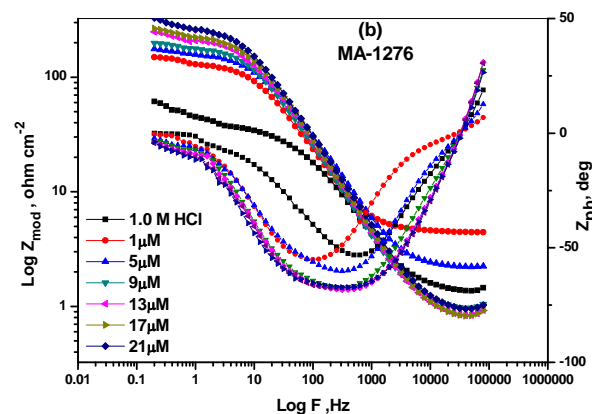
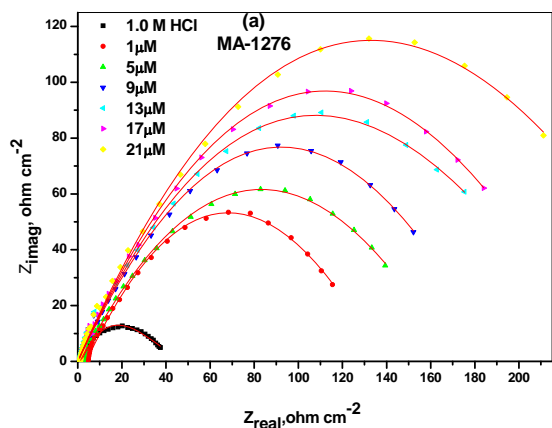
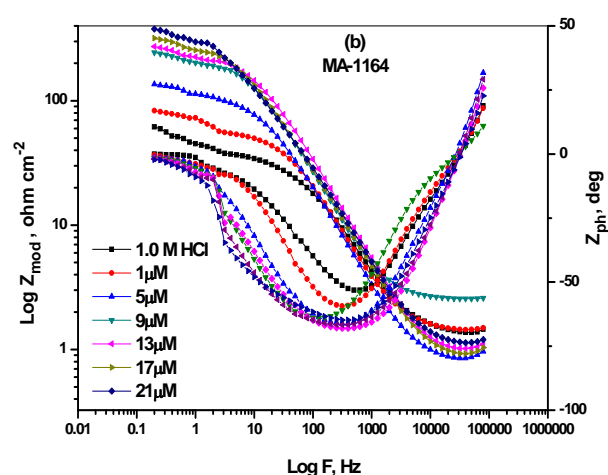
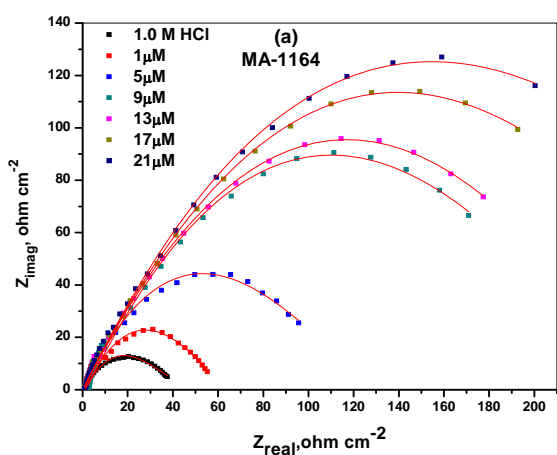
Table 7: EFM and EIS kinetic parameters for CS dissolution in 1.0 M HCl without and with different concentrations of (AZFD) at 298 K

Conc., μM	EFM							EIS		
	i_{corr} (μAcm^{-2})	β_{a} (mV dec^{-1})	β_{c} (mV dec^{-1})	C_{R} (mpy)	CF-2	CF-3	% ϵ_{EFM}	R_{ct} (Ωcm^2)	C_{dl} (μFcm^{-2})	% ϵ_{EIS}
Blank	413.5	91	143	234.6	1.90	2.85	-----	36.4	781	-----
MA-1164										
1	140.4	96	114	79.76	1.81	3.15	66.0	115.1	91.2	68.3
5	138.2	93	110	78.36	2.13	2.88	66.6	148.4	89.8	75.4
9	132.8	98	119	75.31	1.86	2.70	67.9	163.1	79.7	77.6
13	95.16	96	99	53.96	1.78	3.16	77.0	192.7	75.8	81.0
17	91.21	81	103	51.85	2.20	3.36	77.9	203.3	72.5	82.0
21	80.51	92	106	45.75	1.80	3.36	80.5	244.4	70.5	85.0
MA-1276										
1	150.5	86	93	85.39	1.44	2.57	63.6	103.4	424	64.7
5	147.8	66	87	83.75	1.63	3.34	64.3	146.2	112	75.0
9	137.5	80	104	78.12	1.75	3.48	66.7	160.0	110	77.2
13	124.1	88	144	70.61	1.87	3.47	69.9	165.0	92.4	77.9
17	122.4	86	100	69.44	1.57	3.05	70.4	176.1	78.1	79.3
21	86.14	84	101	48.80	1.81	3.43	79.2	208.9	74.7	82.5
MA-1117										
1	226.5	75	84	128.56	1.69	3.35	45.2	70.2	640	48.0
5	168.8	99	113	95.72	1.78	2.79	59.2	110.6	486	67.0
9	149.7	92	110	84.93	1.62	3.29	63.8	135.5	334	73.0
13	135	80	101	76.48	1.83	3.11	67.4	151.5	155	75.9
17	128.7	74	97	72.96	1.86	3.37	68.9	160.5	80	77.2
21	88.06	68	98	49.97	1.92	3.26	78.7	183.3	78.6	80.1

3.3.3. EIS measurements: EIS spectra of CS dissolution in test solution without and with various concentrations of (AZFD) are represented in **Figure 7**. A single depressed capacitive semicircle in inhibited and uninhibited solution is shown in the Nyquist graphs (**Figure 7a**), having one capacitive time constant in the Bode phase graphs (**Figure 7b**). These depressed semicircles are attributed to heterogeneities of the metal surface, roughness, mass transport and adsorption-desorption mode of the (AZFD) molecules at CS/solution interface. The shape of the semicircle in **Figure 7a** not changed in uninhibited and inhibited solutions. These indicate that, the addition of inhibitors for the test medium does not change the corrosion reaction mechanism. But, the diameter of capacitive loop in the existence of inhibitor is wider than that in the blank medium and increases with increase in (AZFD) concentrations. This suggested that the investigated derivatives protect the surface of CS from attack of acid and the (% ϵ_{EIS}) is improved at higher concentration of inhibitor. EIS spectra fitted using the electrical equivalent circuit is given in the **Figure 8**, and then the kinetic parameters were recorded in **Table 7**. The (% ϵ_{EIS}) are obtained using the following relation²⁴:

$$\% \mathcal{E}_{\mathcal{E}} = \left(\frac{R_{ct} - R_{ct}^*}{R_{ct}} \right) \times 100 \quad (11)$$

where R_{ct}^* and R_{ct} is the charge transfer resistance for CS in test solution without and with inhibitor. As shown in **Table 7**, the increase in inhibitor concentrations causes the increase in R_{ct} values and decrease in C_{dl} values. This is attributed to the adsorption of (AZFD) molecules on the CS/solution interface instead of H_2O molecules forming a protective adsorbed film on the CS surface, which lead to increase the electric double layer or reduce the dielectric constant. And therefore, reduces the electron transfer and metal corrosion action²⁵. The results calculated from EIS method were in agreement with pervious ML, AAS, PP and EFM methods.



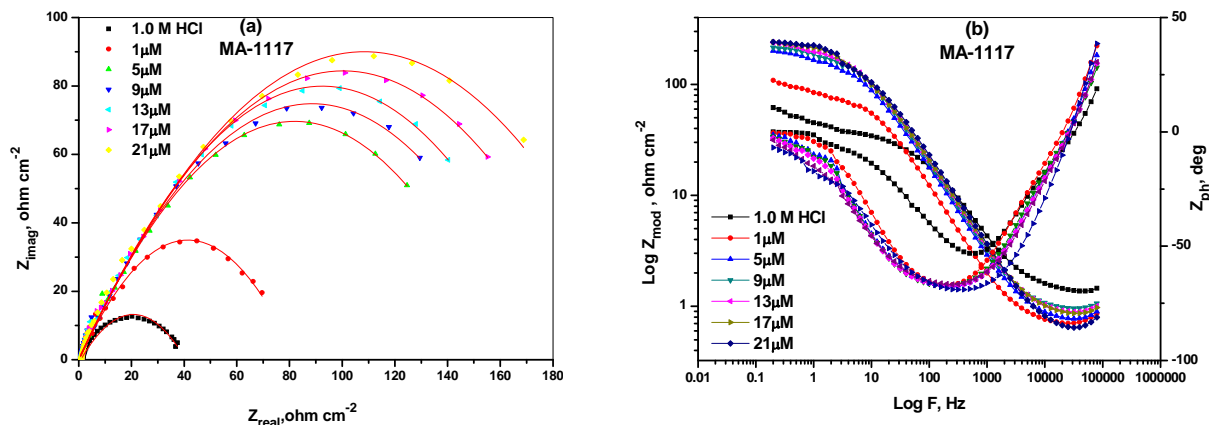


Fig. 7: EIS spectra of CS dissolution in 1.0 M HCl solution in the absence and presence of different concentration of (AZFD) at 298 K. (Nyquist plots (a) and Bode plots (b))

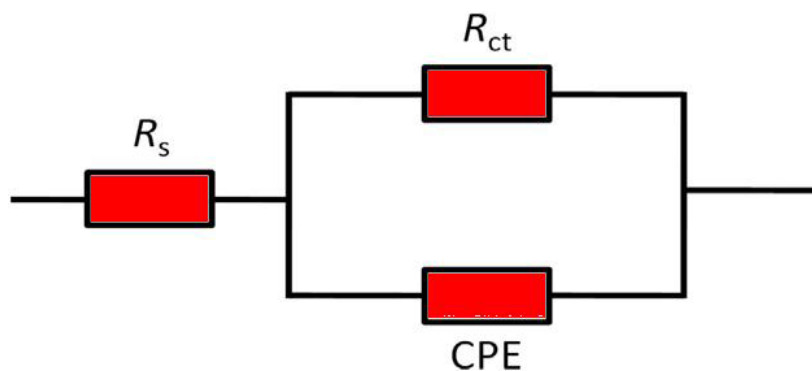


Fig.8: Equivalent circuit used to fit the impedance spectra

3.4. CS surface characterization

3.4.1. AFM analysis: AFM technique is proceeded to investigate the surface morphology of CS in test solution without and with (AZFD). **Figure 9(a–e)** show AFM images for the fresh, blank and inhibited specimen of CS, respectively. The surface roughness obtained for fresh CS coupon is 52 nm (**Figure 9a**). The surface roughness of CS coupon is increased to 590 nm after immersed in test solution (**Figure 9b**). On the contrary, the inhibited solution in the presence of MA-1164, MA-1276 and MA-1117 (**Figure 9c–e**) show reduced in the roughness values to 115, 119 and 125 nm, respectively. This is due to the adsorbed layer of (AZFD) molecules formed on the surface of metal which impedes the dissolution of CS in the aggressive medium. Hence, reliable morphology and smooth was achieved in inhibited CS surface²⁶.

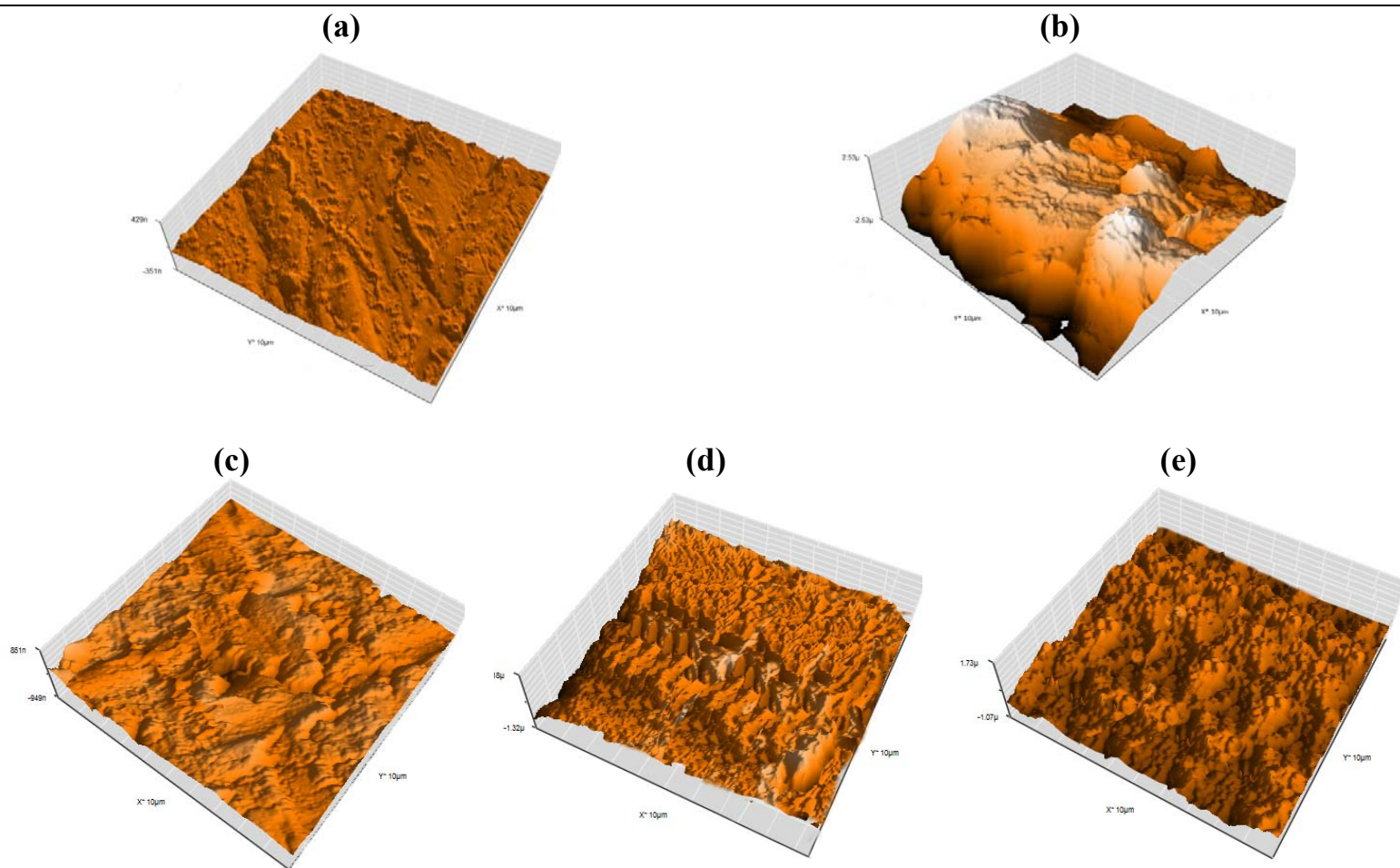


Fig. 9. AFM 3D images for CS surface (a) before, (b) after immersion for 24 h in 1.0 M HCl solution and (c) 1.0 M HCl solution contains 21 μ M of MA-1164 (d) MA-1276 (e) MA-1117

3.4.2. ATR-FTIR and UV/ visible spectral analysis: ATR-FTIR spectroscopy is a powerful technique that identifies functional groups present in various compounds¹⁹. ATR-FTIR spectra of the (AZFD) and the protective layer formed on CS surface exposed to test solution containing (AZFD) are represented in **Figure 10**. As shown from **Figure 10** for *p*-methoxy phenylazafuramide inhibitor (MA-1164), the peaks found at 3235 and 3447 cm^{-1} are characteristic for stretching vibrations of N-H bond for NH_2 and NH, while peaks at 1602, 1628, 1664 cm^{-1} are characteristic for stretching vibrations of C=C, C=N stretching vibrations, and bending vibrations of N-H bond for NH_2 and NH groups. On the other hand, the IR spectra of the protective layer formed on CS surface showed broad band with shift in the wavenumber to 1640 cm^{-1} . The peaks of N-H bond for NH_2 and NH groups become broad peaks. This confirms the adsorption mode of the azafuramide inhibitors on CS surface occurs via binding interaction through these groups, and hence forms a shielding layer against the penetration of water molecules and the corrosive ions to surface of CS¹⁹. Similar patterns have been recorded for MA-1276 and MA-1117.

UV/visible spectra of (AZFD)solution and the test solution containing (AZFD)solution after 24 h of immersion of CS coupons are shown in **Figure 11**. From UV/visible spectra, all the inhibitors showed a band at 386 nm, due to $n-\pi^*$ transition¹¹. On the other hand, the spectra of test solution containing inhibitor molecules after 24 h of immersion of CS samples showed two bands at 316 and 361 nm which attributed to $n-\pi^*$ transition of coordinated and free donor groups of inhibitor, respectively. The possibility of the formation of complex between the dissolved metal ions and the (AZFD) molecules, due to the difference obtained in the absorption spectral after the immersion of CSSample in the corrosive test solution^{27,28}.

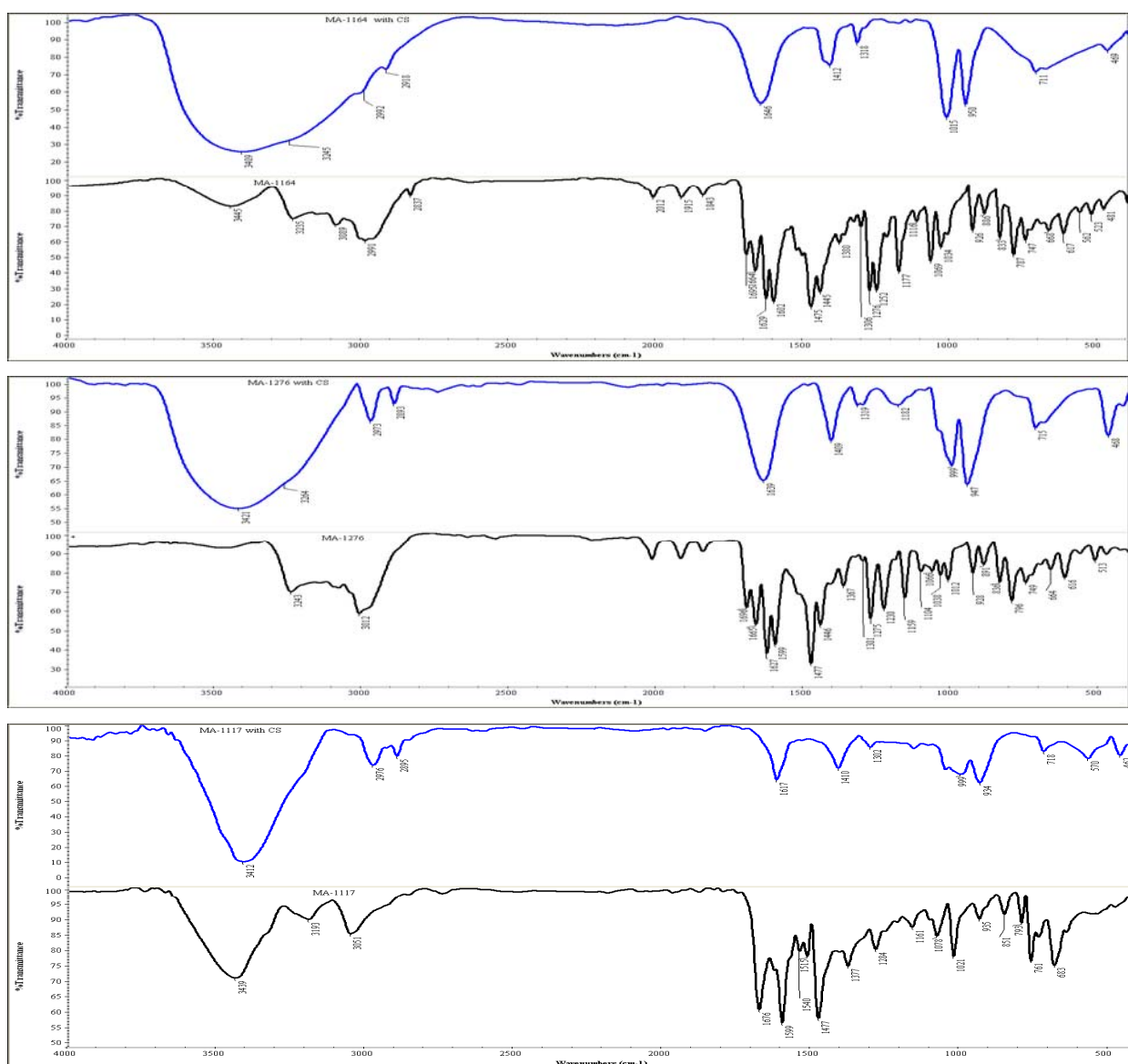


Fig. 10: ATR-FTIR spectra for (AZFD) (a) and the CS surface after immersion in 1.0 M HCl solution containing 21 μ M of (AZFD) (b)

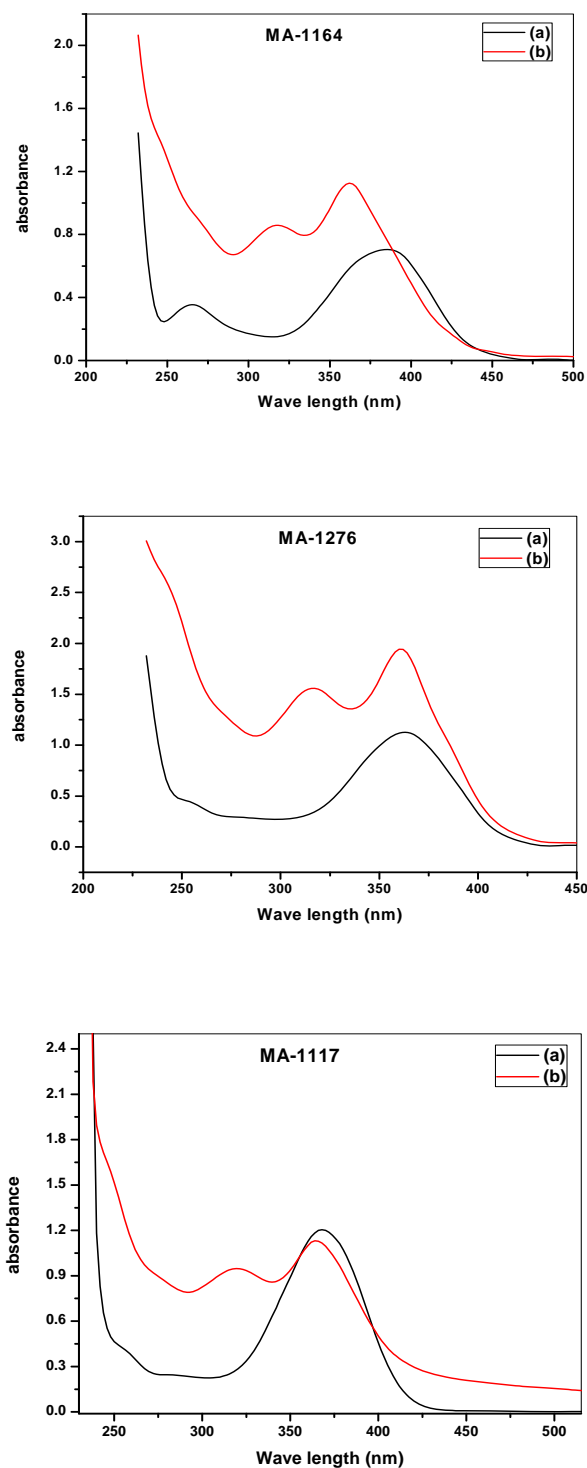


Fig. 11:UV/visible spectra of (AZFD)solution (a) and the test solution containing (AZFD) solution after 24 h of immersion of CS coupons (b)

3.5. Quantum chemical calculations: The inhibition behavior of the investigated (AZFD) for CS corrosion in acidic solution could be discussed by quantum chemical studies using DFT method. The optimized geometry, frontier molecular orbital of HOMO, LUMO and the distribution of Mulliken charge of (AZFD) are plotted in **Figure 12**, respectively. It is seen that, the distributions of electron density were localized on HOMO and LUMO of inhibitors confirms the electron donating and accepting centers are possible in (AZFD) molecules. The detailed data of quantum chemical parameters for (AZFD) are calculated and listed in **Table 8**.

Table 8: Quantum chemical parameters for (AZFD) obtained by DFT method

	MA-1164	MA-1276	MA-1117
$E_{\text{HOMO}} / (\text{eV})$	-5.411	-5.302	-5.214
$E_{\text{LUMO}} / (\text{eV})$	-4.122	-3.968	-3.768
$\Delta E (E_{\text{LUMO}} - E_{\text{HOMO}}) / (\text{eV})$	1.289	1.334	1.446
$\chi_{\text{inh}} / (\text{eV/mol})$	4.766	4.635	4.491
$\eta_{\text{inh}} / (\text{eV/mol})$	0.640	0.670	0.720
ΔN	1.740	1.770	1.740
Mulliken charge analysis			
N(4)	-0.418	-0.179	-0.165
N(19)	-0.772	-0.191	-0.908
N(20)	-0.505	-0.616	-0.631
O(8)	-0.346	-0.732	-----
O(21)	-0.124	-----	-----
F(21)	-----	-0.230	-----

According to the frontier molecular orbital theory (FMO), the inhibition efficiency of investigated inhibitors for CS corrosion in acidic solution is related to the energy of lowest unoccupied molecular orbital (E_{LUMO}), the energy of highest occupied molecular orbital (E_{HOMO}) and the energy gap ΔE ($\Delta E = E_{\text{LUMO}} - E_{\text{HOMO}}$)²⁹. From the Table 8, it can be noted that, the higher E_{HOMO} values indicate that (AZFD) molecules can easily give electrons to the empty d-orbital of iron. But, the lower E_{LUMO} values show a higher electron accepting ability from the CS metal. The smaller values of ΔE show the stability of formed complex on the CS surface which determines the soft-soft interaction between the soft metal acid and the soft base inhibitor in the investigated system³⁰. Therefore, the reactivity order of (AZFD) for corrosion inhibition of CS according to ΔE is MA-1164 > MA-1276 > MA-1117. The value of ΔN clarifies the number of electrons transferred from the (AZFD) molecules to the surface of metal. When ΔN is lower than 3.6, this means that the (%) of (AZFD) molecules increases with the increase of electron donating ability at the CS surface. ΔN is calculated as the following relation:

$$\Delta N = \frac{\chi_{\text{Fe}} - \chi_{\text{inh}}}{2(\eta_{\text{Fe}} + \eta_{\text{inh}})} \quad (12)$$

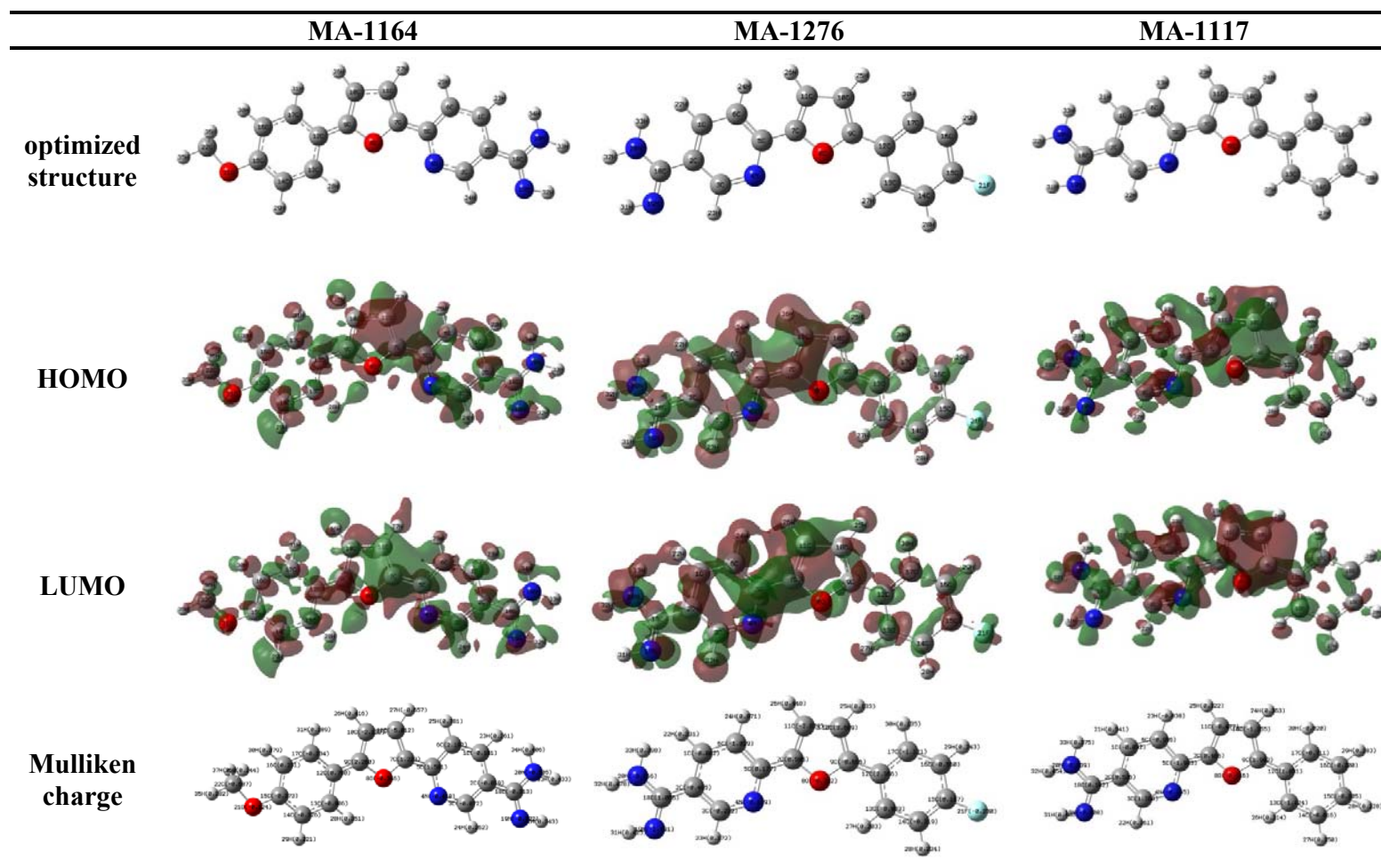
Where χ_{inh} and η_{inh} are the absolute electronegativity and the absolute hardness the (AZFD) molecules, respectively and they are calculated as follow taking into consideration that the theoretical values of χ_{Fe} and η_{Fe} for Fe are (7.0 and 0.0 eV/mol), respectively:

$$\chi = -\frac{1}{2} (E_{\text{LUMO}} + E_{\text{HUMO}}) \quad (13)$$

$$\eta = -\frac{1}{2} (E_{\text{LUMO}} - E_{\text{HUMO}}) \quad (14)$$

As shown in Table 8, it can be noted that, ΔN values for three (AZFD) are < 3.6 ; this indicates that the inhibition effect resulted from the electrons donation to the vacant d- orbital of metal³¹. The Mulliken charge distributions of atoms for the investigated azafuramidines derivatives obtained by DFT calculations are shown **Figure 12**. It is deduced that the more negative charge on heteroatoms, the more easily electrons donation and electrostatic attraction between the (AZFD) molecules and the CS surface. It is clear that from **Figure 12**, the most of the negative charge exist on the N(4), N(19), N(20), O(8), O(21), F(21) atoms for (AZFD). Therefore, these heteroatoms act as the active sites for the adsorption of (AZFD) molecules on the metal surface. From the quantum chemical analysis, it is found that, an agreement with the previously mentioned experimental data obtained by ML, ASS, PP, EFM, EIS measurements.

Fig.12:The optimized structure, HOMO, LUMO orbitals and Mulliken charge for (AZFD)obtained by DFT method



3.6. Mechanism of corrosion inhibition: The inhibition mechanism of CS corrosion in acidic media using the investigated azafuramidines molecules can be discussed on the basis of molecular adsorption. These inhibitors inhibit the corrosion of CS by controlling the cathodic and anodic reactions sites. According to, the adsorption isotherm, the inhibitors molecules were adsorbed chemically on the surface of CS. The (AZFD) molecules could be easily protonated in acidic solution, because of high electron density on it, and adsorbed on the cathodic centers of the CS and reduce the hydrogen evolution. On the other hand, the adsorption on anodic sites occurs via π -electrons of aromatic rings and unshared electron pairs on (O, N) heteroatoms exist in the investigated (AZFD) which reduce the anodic dissolution of CS

32

CONCLUSION

(AZFD) act as good inhibitors for CS in acidic medium and inhibition efficiency increased with the increase of inhibitor concentrations. The adsorption of (AZFD) on CS surface obeys Langmuir adsorption isotherm. The corrosion current density reduced as the concentration of (AZFD) increased indicated that inhibitor acted as (mixed-type) inhibitor. The C_{dl} values decreased when increasing the concentrations of inhibitor concentrations. This is attributed to the adsorption of (AZFD) molecules at the CS/ solution interface. The surface investigation using AFM showed a reduction of CS corrosion by formation of adsorbed layer onto the surface. ATR-FTIR and UV/visible spectra, confirmed the bond formation of the (AZFD) with CS. Quantum chemical calculations supported the experimental data and pointed out that the order of inhibition efficiency, for (AZFD), is the following: MA-1164 > MA-1276 > MA-1117.

REFERENCES

1. L. Guo, S. Kaya, I. B. Obo, X. Zheng, Y. Qiang, Toward understanding the anticorrosive mechanism of some thiourea derivatives for carbon steel corrosion: A combined DFT and molecular dynamics investigation, *Journal of Colloid and Interface Science*, 2017, 506, 478–485.
2. S. E. Kaskah, M. Pfeiffer, H. Klock, H. Bergen, G. Ehrenhaft, P. Ferreirab, J. Gollnick, C. B. Fischer, Surface protection of low carbon steel with N-acyl sarcosine derivatives as green corrosion inhibitors, *Surfaces and Interfaces*, 2017, 9, 70–78.
3. T. Pojtanabuntoeng, M. Salasi, An electrochemical study of carbon steel CO₂ corrosion in the presence of monoethylene glycol: The effects of pH and hydrodynamic conditions, *Electrochimica Acta*, 2017, 258, 442 – 452.
4. M. A. Deyab, M. T. Zaky, M. I. Nessim, Inhibition of acid corrosion of carbon steel using four imidazolium tetrafluoroborates ionic liquids, *Journal of Molecular Liquids*, 2017, 229, 396–404.
5. P. Morales-Gil, M.S. Walczak, C. R. Camargo, R. A. Cottis, J. M. Romero, R. Lindsay, Corrosion inhibition of carbon-steel with 2-mercaptobenzimidazole in hydrochloric acid, *Corrosion Science*, 2015, 101, 47–55.

6. M. N. El-Haddad, A. S. Fouda, Inhibition Effect and Adsorption Behavior of New Azodye Derivatives on Corrosion of Carbon Steel in Acid Medium, *Journal of Dispersion Science and Technology*, 2013, 34, 1471–1480.
7. S. Öztürk, Synthesis and Corrosion Inhibition Effects of Quinazolin-(3H)-4- One Derivatives Containing Long-Chain Pyridinium Salts on Carbon Steel in 1.5 M HCl, *Protection of Metals and Physical Chemistry of Surfaces*, 2017, 53, 920–927.
8. V. P. Raphael, K. J. Thomas, K. S. Shaju, A. Paul, Corrosion inhibition investigations of 3-acetylpyridine semicarbazone on carbon steel in hydrochloric acid medium, *Res. Chem. Intermed.*, 2014, 40, 2689–2701.
9. M. T. Alhaffar, S. A. Umoren, I. B. Obot, S. A. Alia, Isoxazolidine derivatives as corrosion inhibitors for low carbon steel in HCl solution: experimental, theoretical and effect of KI studies, *RSC Adv.*, 2018, 8, 1764–1777.
10. M. A. Deyab, A. S. Fouda, M. M. Osmana, S. Abdel-Fattah, Mitigation of acid corrosion on carbon steel by novel pyrazolone derivatives, *RSC Adv.*, 2017, 7, 45232–45240.
11. M. A. Hegazy, S. S. Abd El Rehim, A. M. Badawia, M. Y. Ahmed, Studying the corrosion inhibition of carbon steel in hydrochloric acid solution by 1-dodecyl-methyl-1H-benzo[d][1,2,3]triazole-1-ium bromide, *RSC Adv.*, 2015, 5, 49070–49079.
12. A. S. Fouda, M. Abdallah, A. Attia, Inhibition of Carbon Steel Corrosion by Some Cyanoacetohydrazide Derivatives in HCl Solution, *Chem. Eng. Comm.*, 2010, 197:1091–1108.
13. A.S. Fouda, M.A. Ismail, A.S. Abousalem, G.Y. EL-Elewady. Experimental and Theoretical Studies on Corrosion Inhibition of 4-Amidinophenyl-2,2'-bifuran and its Analogues in acidic solutions, *RSC Advances*, 2017, 7, 46414–46430.
14. M.M. Youssef, R. K. Arafa and M.A. Ismail, drug design, development and therapy, 10, (2016)1133–1146.
15. K. Krishnaveni, K. Sampath, J. Ravichandran, C. Jayabalakrishnan, N-methyl-2-(2-nitrobenzylidene) hydrazine carbothioamide - A new corrosion inhibitor for mild steel in 1 molL⁻¹ hydrochloric acid, *Chinese Journal of Chemical Engineering*, 2015, 23, 1916–1922.
16. P. Roy, S. Kr. Saha, P. Banerjee, S. Dey, D. Sukul, Experimental and theoretical investigation towards anti-corrosive property of glutamic acid and poly-c-glutamic acid for mild steel in 1 M HCl: intramolecular synergism due to copolymerization, *Res. Chem. Intermed.*, 2017, 43, 4423–4444.
17. F. E. Heakal, M. A. Deyabb, M. M. Osman, A. E. Elkholy, Performance of Centaurea cyanus aqueous extract towards corrosion mitigation of carbon steel in saline formation water, *Desalination*, 2018, 425, 111–122.

18. N. J. N. Nnaji, O. T. Ujam, N. E. Ibisi, J. U. Ani, T. O. Onuegbu, L. O. Olasunkanmi, E. E. Ebenso, Morpholine and piperazine based carboxamide derivatives as corrosion inhibitors of mild steel in HCl medium, *J. Mol. Liq.*, 2017, 230, 652–661.
19. A. S. Fouda, M.A. Ismail, G.Y. Elewady, A.S. Abousalem, Evaluation of 4-amidinophenyl-2,2'-bithiophene and its aza-analogue as novel corrosion inhibitors for CS in acidic media: Experimental and theoretical study, *Journal of Molecular Liquids*, 2017, 240, 372–388.
20. H. Bentrach, Y. Rahali, A. Chala, Gum Arabic as an eco-friendly inhibitor for API 5L X42 pipeline steel in HCl medium, *Corros. Sci.*, 2014, 82, 426–431.
21. M. N. El-Haddad, A. S. Fouda, H.A. Mostafa, Corrosion Inhibition of Carbon Steel by New Thiophene Azo Dye Derivatives in Acidic Solution, *JMEPEG*, 2013, 22, 2277–2287.
22. M. N. El-Haddad, Inhibitive action and adsorption behavior of cefotaxime drug at copper/hydrochloric acid interface: electrochemical, surface and quantum chemical studies, *RSC Adv.*, 2016, 6, 57844– 57853.
23. Y. Kharbach, F. Z. Qachchachi, A. Haoudi, M. Tourabi, A. Zarrouk, C. Jama, L .O. Olasunkanmi, E. E. Ebenso, F. Bentiss, Anticorrosion performance of three newly synthesized isatin derivatives on carbon steel in hydrochloric acid pickling environment: Electrochemical, surface and theoretical studies, *Journal of Molecular Liquids*, 2017, 246, 302–316.
24. M. A. Deyab, S. T. Keera, On corrosion and corrosion inhibition of carbon steel in stored biodiesel: electrochemical (AC and DC) studies, *Journal of the Taiwan Institute of Chemical Engineers*, 2016, 68, 187–191.
25. M. Bouanis, M. Tourabi, A. Nyassi, A. Zarrouk, C. Jama, F. Bentissa Corrosion inhibition performance of 2,5-bis(4-dimethylaminophenyl)-1,3,4-oxadiazole for carbon steel in HCl solution: Gravimetric, electrochemical and XPS studies, *Applied Surface Science*, 2016, 389, 952–966.
26. P. Kannan, T. S. Rao, N. Rajendran, Improvement in the corrosion resistance of carbon steel in acidic condition using naphthalen-2-yl-naphthalene-2-carboxamide inhibitor, *Journal of Colloid and Interface Science*, 2018, 512, 618–628.
27. Y. Guo, B. Xu, Y. Liu, W. Yang, X. Yin, Y. Chen, J. Le, Z. Chen, Corrosion inhibition properties of two imidazolium ionic liquids with hydrophilic tetrafluoroborate and hydrophobic hexafluorophosphate anions in acid medium, *Journal of Industrial and Engineering Chemistry*, 2017, 56, 234–247.
28. M. El Faydy, M. Galai, M. Ebn Touhami, I. B. Obot, B. Lakhri, A. Zarrouk, Anticorrosion potential of some 5-amino-8-hydroxyquinolines derivatives on carbon steel in hydrochloric acid solution: Gravimetric, electrochemical, surface morphological, UV–visible, DFT and Monte Carlo simulations, *Journal of Molecular Liquids*, 2017, 248, 1014–1027.

29. Neeraj Kumar Gupta,a Chandrabhan Verma,ab R. Salghi,c H. Lgaz,cd A. K. Mukherjeea and M. A. Quraishi, New phosphonate based corrosion inhibitors for mild steel in hydrochloric acid useful for industrial pickling processes: experimental and theoretical approach†, Cite this: New J. Chem., 2017, 41, 13114 -1329.
30. Yishan Wang, Yu Zuo, The adsorption and inhibition behavior of two organic inhibitors for carbon steel in simulated concrete pore solution, Corrosion Science, 2017, 118, 24–30.
31. Jabir H. Al-Fahemi a, M. Abdallah , Elshafie A.M. Gad, B.A.A.L. Jahdaly, Experimental and theoretical approach studies for melatonin drug as safely corrosion inhibitors for carbon steel using DFT, Journal of Molecular Liquids, 2016, 222, 1157–1163.
32. Ahmed A. Farag, A. S. Ismail, M. A. Migahed, Inhibition of carbon steel corrosion in acidic solution using some newly polyester derivatives, Journal of Molecular Liquids, 2015, 211, 915–923.

Corresponding author: Mahmoud N. EL-Haddad

Chemistry Department, Faculty of Science, Mansoura University, Mansoura-35516, Egypt

noaman_eg@yahoo.com; asfouda@mans.edu.eg

Online publication Date: 28.07.2018